10-2016

Impact of Upper-Tropospheric Temperature Anomalies and Vertical Wind Shear on Tropical Cyclone Evolution Using an Idealized Version of the Operational GFDL Hurricane Model

Robert E. Tuleya
Old Dominion University

Morris Bender

Thomas R. Knutson

Joseph R. Sirutis

Biju Thomas

See next page for additional authors

Original Publication Citation

Tuleya, R. E., Bender, M., Knutson, T. R., Sirutis, J. J., Thomas, B., & Ginis, I. (2016). Impact of upper-tropospheric temperature anomalies and vertical wind shear on tropical cyclone evolution using an idealized version of the operational gfdl hurricane model. *Journal of the Atmospheric Sciences, 73*(10), 3803-3820. doi:10.1175/jas-d-16-0045.1

Impact of Upper-Tropospheric Temperature Anomalies and Vertical Wind Shear on Tropical Cyclone Evolution Using an Idealized Version of the Operational GFDL Hurricane Model

ROBERT E. TULEYA

Center for Coastal Physical Oceanography, Old Dominion University, Norfolk, Virginia

MORRIS BENDER, THOMAS R. KNUTSON, AND JOSEPH J. SIRUTIS

NOAA/Geophysical Fluid Dynamics Laboratory, Princeton, New Jersey

BIJU THOMAS AND ISAAC GINIS

Graduate School of Oceanography, University of Rhode Island, Narragansett, Rhode Island

(Manuscript received 30 January 2016, in final form 1 June 2016)

ABSTRACT

The GFDL hurricane modeling system, initiated in the 1970s, has progressed from a research tool to an operational system over four decades. This system is still in use today in research and operations, and its evolution will be briefly described. This study used an idealized version of the 2014 GFDL model to test its sensitivity across a wide range of three environmental factors that are often identified as key factors in tropical cyclone (TC) evolution: SST, atmospheric stability (upper-air thermal anomalies), and vertical wind shear (westerly through easterly). A wide range of minimum central pressure intensities resulted (905–980 hPa). The results confirm that a scenario (e.g., global warming) in which the upper troposphere warms relative to the surface will have less TC intensification than one with a uniform warming with height. The TC rainfall is also investigated for the SST–stability parameter space. Rainfall increases for combinations of SST increase and increasing stability similar to global warming scenarios, consistent with climate change TC downscaling studies with the GFDL model. The forecast system's sensitivity to vertical shear was also investigated. The idealized model simulations showed weak disturbances dissipating under strong easterly and westerly shear of $10\,\mathrm{m\,s^{-1}}$. A small bias for greater intensity under easterly sheared versus westerly sheared environments was found at lower values of SST. The impact of vertical shear on intensity was different when a strong vortex was used in the simulations. In this case, none of the initial disturbances weakened, and most intensified to some extent.

1. Introduction

The GFDL hurricane modeling system is a multidecade project initiated in the 1970s during the early years of numerical weather prediction, when it became clear that global models might have limitations in simulating mesoscale systems. The GFDL model was one of the first 3D regional models developed, and the foremost research hurricane model when developed for process studies (Kurihara and Tuleya 1974). During the next two decades, it gradually became more sophisticated, with more realistic initial and boundary conditions and land processes and the development of the moveable, nested grid system (Kurihara et al. 1979), still unique and in use today in research and operations. Because of its capabilities, it was transitioned into NCEP (1995) and U.S. Navy (1996) operational suites. Besides real-data forecasts and process studies, it also became a valuable tool for climate studies (e.g., Knutson et al. 1998; Bender et al. 2010).

An idealized framework will be used to explore the current model's sensitivity to basic atmospheric parameters that are often attributed as factors in storm evolution: SST, atmospheric stability, and vertical wind shear. Idealized studies have been used by the GFDL model and other hurricane models to focus on processes

Corresponding author address: Robert E. Tuleya, Center for Coastal Physical Oceanography, Innovation Park Research Building 1, 4111 Monarch Way, 3rd Floor, Norfolk, VA 23508.
E-mail: robert.tuleya@noaa.gov

DOI: 10.1175/JAS-D-16-0045.1

obscured by synoptic fluctuations. They can explore model strengths and weaknesses when simulating isolated tropical cyclone (TC) processes but may have limitations in assessing complicated phenomena. They may fail to assess the predictability of particular phenomena, such as hurricane track and intensity.

An earlier version of the GFDL model has been used previously to study some of these factors (Shen et al. 2000, hereafter SH00), and one may consider this paper as a follow on to that study, in which atmospheric stability and SST sensitivity were studied in detail. Atmospheric stability is a known factor (e.g., Gray1968, 1998) in tropical cyclone intensification and has been studied by Cheung (2004) and DeMaria et al. (2001). This paper will also investigate the effect on stability and SST on TC rainfall. Finally, we will investigate the sensitivity of modeled TC intensity to vertical wind shear. Vertical wind shear has not be studied systematically in the GFDL model since basic model studies in the 1980s, which used a much earlier research version of the model. Empirically, vertical wind shear has been known to effect TC intensity [e.g., review of Nolan and McGauley (2012)] but it has been somewhat problematic to model in both the idealized and real environment. Previous studies by Frank and Ritchie (2001, 2002), Wong and Chan (2004, hereafter WC04), and Ritchie and Frank (2007) have studied the impacts of vertical shear on idealized storms. Some idealized model runs have been performed with the Hurricane Weather Research and Forecasting (HWRF) system (Gopalakrishnan et al. 2011), but effects of vertical shear have not been reported. Other WRF Model experiments have been performed as well (Nolan and McGauley 2012). Operational model sensitivity has not been studied extensively, except through some empirical analyses comparing dynamical model results to observations and to empirical statistical models that use shear as predictors. Our experience with operational predictions is that early versions of the model were not as sensitive to shear as observed storms. Over the years, the model has been upgraded with the major goal of improving track and intensity prediction. This study will therefore examine how the 2014 version of the operational hurricane model responds to basic meteorological parameters across systematic parameter spaces with varying SSTs, stability, and vertical shear—three key factors that drive TC behavior.

2. GFDL model evolution since 2000

The GFDL model and forecast system has been a dynamic system undergoing change and improvements from its inception in the 1980s to its current state. Kurihara et al. (1998) described the model in its first year of operational implementation, while Bender et al. (2007) summarized the improvements and the resulting performance during the first decade of operational implementation. It is informative to present the more recent changes to this operationally important hurricane system. Table 1 summarizes the evolution of the model changes since 2000 and contrasts the model architecture of ~2000 to that of the 2014 model. One of the most straightforward changes in the 2000s was the increase in both vertical and horizontal resolution. The inner nest resolution increased from 1/6° to 1/8°, and the number of vertical levels has increased from 18 to 42. To make the GFDL hurricane model more compatible with the improving tropical forecasts of the NCEP Global Forecast System (GFS), multiple changes were made to the physics packages of the GFDL model, including the transition to GFS physics packages [nonlocal boundary layer and simplified Arakawa–Schubert (SAS) convection parameterizations] in 2003. On the other hand, improvements, such as bulk microphysics, were introduced to the GFDL model in 2006 to simulate more realistic small scales. Since 2000, surface physics have been adjusted, reducing surface drag initially and subsequently making several modifications to the surface heat and moisture fluxes. In hindsight and in light of more recent observations, surface heat and moisture fluxes were kept artificially high to maintain strong 10-m winds in the early operational years of the GFDL model. As computer power improved dramatically, increased resolution was more viable, and since observational trends indicated smaller energy and drag exchange at the surface, surface exchange coefficients were reduced. Despite these adjustments, the surface energy exchange at the ocean is still an unresolved issue for hurricane conditions. Ocean coupling was added in 2001 with the inclusion of the University of Rhode Island (URI) version of the Princeton Ocean Model (POM) with other minor ocean model changes through the various model versions. Coupling to a new message passing interface–enabled version of POM (MPIPOM) was made operational in 2014, with improved ocean physics and increased horizontal resolution in the ocean from 1/6° to 1/12° (Yablonsky et al. 2015b).

The GFDL model storms, in our assessment, have gradually become more realistic in evolution and structure. A description of more recent changes after 2010 is found in McClung (2012; http://www.nws.noaa.gov/os/notification/tin12-18gfdl_aaa.htm). The version of the model used in the present study is the GFDL 2014 system, which includes the following changes: an inner nest resolution increase from 1/12° to 1/18°, inclusion of 3D advection of all individual microphysical condensates, and the introduction of the

TABLE 1. GFDL operational hurricane model evolution from 2000 to 2014.

	GFDL 2000	GFDL 2014
Grid configuration	Three nests (1°, 1/3°, 1/6°) 18 levels	Three nests (1/2°, 1/6°, 1/18°) 42 levels
Ocean coupling	None	MPIPOM-TC
Convective parameterization	Kurihara convective adjustment	SAS with momentum mixing
Explicit condensation	Large-scale condensation	Ferrier 3D advection of condensates
Boundary layer	Based on Mellor–Yamada 2.0	GFS nonlocal
Surface layer	GFDL (CH = CD, where CH and CD are surface heat and momentum exchange coefficients, respectively)	GFDL updated (CH < CD; both less than GFDL 2000)
Land surface model	GFDL slab	GFDL slab
Dissipative heating	None	Based on Zhang and Altshuler (1999)
Radiation	GFDL	GFDL

MPIPOM-TC. In addition, surface flux coefficients were further reduced, with surface fluxes accounting for ocean current magnitude relative to low-level wind.

As shown in Fig. 1, the GFDL operational hurricane model has made some progress in TC intensity prediction, with the above-stated model upgrades apparently responsible. Forecast intensity error at 48-h lead time has, on average, decreased from ~22 knots (~11 m s^{-1}) in 2000 to ~14 knots (~7 m s^{-1}) in 2014. Other forecast lead times display a similar tendency. Note, however, that there is considerable year-to-year variability in these error metrics as a result of variations in forecast predictability, storm number inhomogeneity, and likely sampling error (noise). The GFDL model's error has tended to become closer to official operational forecast error, which also supports the conclusion that the model has improved over time. NHC forecasts use intensity forecast guidance from several sources, with the empirical products still highly regarded. TC track forecasts have improved even more dramatically, in percentage terms, than TC intensity (not shown). One would assume that these improvements would also lead to better storm representations for real-time forecasts as well as increasingly realistic behavior of TCs in global warming sensitivity studies.

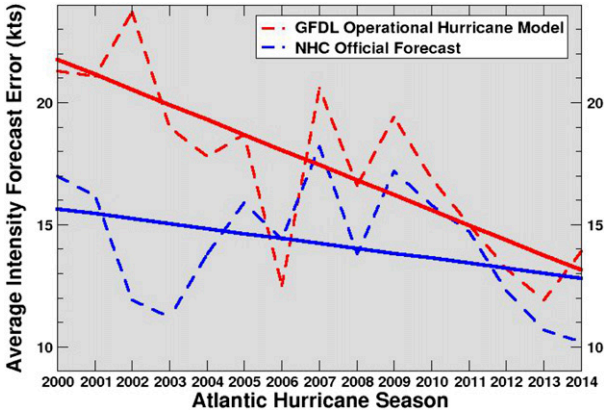

FIG. 1. GFDL operational hurricane model 48-h intensity error (red) from 2000 to 2014. NHC official forecast error is also shown (blue), which utilized multiple guidance models, including the GFDL model. Solid lines are linearly regressed trends obtained for individual years.

3. Experimental design

Our experiments used the same model domain setup as in Knutson et al. (2015) with a range of 105°W–10°E and 0°–50°N. In the present study, the domain is covered with ocean conditions everywhere. The experimental initial conditions were patterned after those of SH00, with nearly identical thermal and relative humidity profiles (Table 2) derived from GARP Atlantic Tropical Experiment (GATE) III observations. A climatological-mean ocean profile for the Atlantic main development region

TABLE 2. GATE control temperature and relative humidity profiles.

Temperature (K)	Relative humidity (%)	Pressure (hPa)
220.5	0.01	20.7
210.1	14.9	74.0
202.1	20.5	124.4
214.6	25.7	174.6
226.5	30.6	224.7
235.8	34.0	274.7
245.0	37.3	324.8
251.8	41.1	374.8
258.0	45.1	424.8
267.0	50.8	497.4
274.3	56.7	593.5
281.2	62.7	688.1
287.1	69.3	777.2
292.1	75.1	856.3
295.9	79.8	920.4
298.1	82.4	960.5
299.3	83.3	981.5
299.7	84.2	995.0

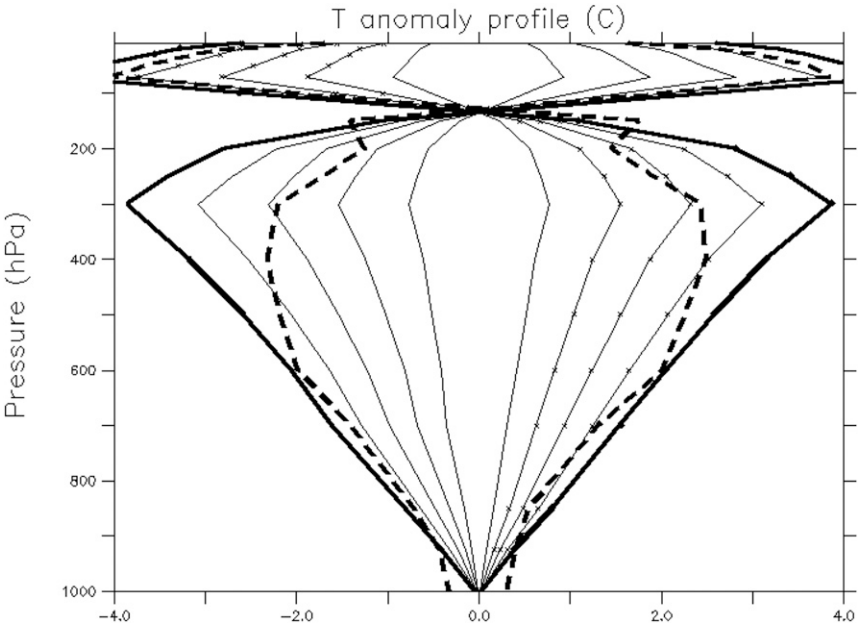

FIG. 2. Vertical distributions of initial temperature anomalies are shown by solid lines. Initial (60 h) values of extreme-case warm and cold upper-troposphere anomalies shown in thick solid (dashed) lines. All values are domain averaged. For each SST case, the same surface air–sea temperature difference and lapse rate dT/dz of the temperature profile is specified for each thermal anomaly from the GATE control.

(MDR) derived from the U.S. Navy Generalized Digital Environmental Model (GDEM) was used for the coupled ocean component, which was based on the URI MPIPOM-TC (Yablonsky et al. 2015b). As in Knutson et al. (2015), when SST anomalies were applied, the ocean thermal profiles were adjusted by a mixing scheme that approximately maintains the original mixed-layer depth and adjusts temperature toward the GDEM climatology beneath the mixed layer, as described in Yablonsky and Ginis (2008). In global warming scenarios, another approach is to use the full ocean temperature change profile from climate models as a function of horizontal location and depth, as in Huang et al. (2015, hereafter H15), or a hybrid of the two approaches, as in Bender et al. (2010). The impact of using these different warmed ocean profiles is explored in the appendix for the idealized framework used in our study.

As in SH00, our basic sensitivity test design consists of a systematic application of 10 atmospheric thermal anomalies aloft shown in Fig. 2 combined in a series of experiments with 10 SST anomalies, resulting in a total of 121 individual experiments (11 × 11, including control experiments). The atmospheric relative humidity is fixed in all experiments to the GATE III observations. An idealized $5\,\mathrm{m\,s^{-1}}$ easterly environmental flow was specified that matched one experimental suite in SH00. A similar specified initial storm vortex (Fig. 3) was also used for direct comparison with SH00. In addition, a weaker specified vortex was applied in additional experiments in order to more properly model the important stage of development from a weak tropical storm to full hurricane development. For each of the experiments, the model was integrated for 5 days.

To test shear sensitivity, a horizontally invariant shear profile of magnitude up to $10\,\mathrm{m\,s^{-1}}$ based on WC04 is applied in a systematically varying set of experiments, with magnitude of shear ranging from $10\,\mathrm{m\,s^{-1}}$ magnitude easterly through zero shear to $10\,\mathrm{m\,s^{-1}}$ westerly shear for the 11 individual experiments. As in the thermal anomaly suite of experiments discussed above, 11 different shear experiments are performed for a range of SSTs. For all experiments, the surface wind field is specified as $5\,\mathrm{m\,s^{-1}}$ easterly flow. With this experimental design, the surface interaction with the ocean is the same initially for all experiments. As in the atmospheric thermal–SST space experiments, two sets of experiments with different specified vortices are performed, with all simulations extending to 5 days regardless of whether the storms in an experiment dissipated. The suite of experiments is quite similar in design to that of Nolan and McGauley (2012) in that surface flow is fixed at $5\,\mathrm{m\,s^{-1}}$ surface easterly, and the vertical shear is systematically changed aloft from easterly to westerly at

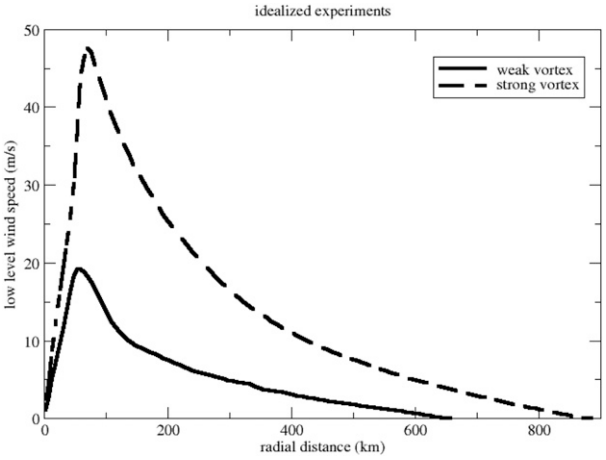

FIG. 3. The two axisymmetric 10-m wind profiles used in this idealized study for the incipient vortex initialization: weak (solid) and strong (dashed) vortex. The strong vortex was similar to that used in SH00 based on Hurricane Fran (2 Sep 1996) at moderate hurricane strength.

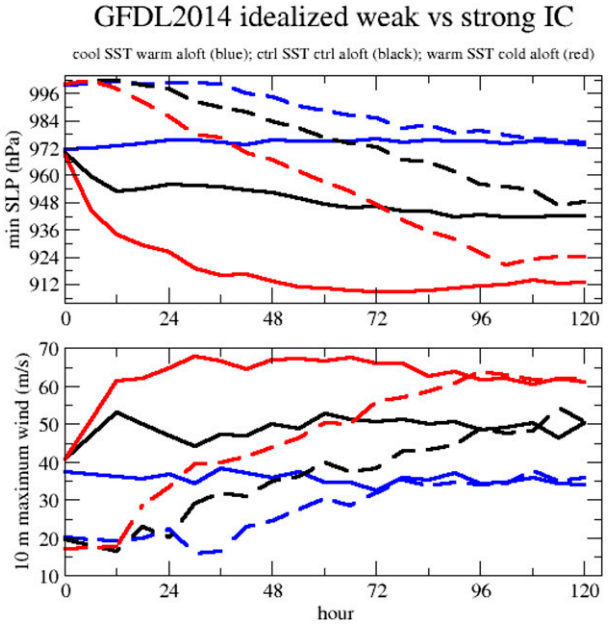

FIG. 4. Time history of (top) model central surface pressure and (bottom) maximum 10-m wind for three different upper-air anomalies at three distinct SST anomalies. The cold SST (−2.5°C)–warm aloft (+3.9°C) case (blue) is the least cyclogenetic combination of anomalies. The warm SST (+2.5°C)–cold aloft (−3.9°C) case (red) is the most cyclogenetic combination of anomalies. The control case (black) has a 0°C SST and no upper-air anomalies. Dashed and solid lines, respectively, denote the weak and strong initial vortex cases.

approximately the same magnitude. The results are shown is section 6.

4. Impacts of SSTs and upper-tropospheric thermal anomalies on intensity

This section will cover the results of impacts on thermal stabilities, including any differences with the results of SH00. Since the initial conditions of the strong specified vortex are almost identical to that of SH00, any substantial differences will presumably be due to the model system evolution (primarily the model physics and resolution). Some differences also exist with the vortex initialization procedure, but these are believed to have a minor influence compared to the model differences themselves. As in SH00 and in the GFDL operational system, the thermal field is free to evolve in time constrained only by the time-independent lateral boundary conditions. In the tropics, there exists a strong constraint to maintain the thermal profile [and the convective available potential energy (CAPE)] to the moist adiabatic one (Emanuel 2007). Nevertheless, SH00 and others (e.g., Williams and Renno 1993) have shown that significant deviations of the tropical thermal profile occur. In the present experimental design, there is a tendency for the initial upper-air thermal anomalies to degrade with time. Figure 2 indicates that this degradation is ~33% after 60 h of integration for the most extreme thermal anomaly cases in the control SST scenario. Nevertheless, significant anomalies are retained, and they affect tropical cyclone intensity in a systematic manner.

a. *Transient behavior of idealized experiments*

The intense specified vortex of 45 m s^{-1} was used to compare more directly with the SH00 study. The weaker specified vortex of 17.5 m s^{-1} allowed for a wider range of storm development scenarios from weak tropical storm to strong hurricane. A representative set of time series is shown in Fig. 4 for both minimum surface pressure and 10-m maximum wind, with three cases for each specified initial vortex. One of the three cases is the control case with the control SST and control Gate III vertical profile. The other two cases represent extreme cases of anomalous environment: warm aloft–cool SST (least cyclogenetic) and cold aloft–warm SST (most cyclogenetic). Note that all weak initial vortex cases are initially at 1000 hPa (~20 m s^{-1}), while the strong vortex cases are initially at 969 hPa (~40 m s^{-1}). The weak and strong vortex cases eventually develop to approximately the same intensity levels for the control and noncyclogenetic (stable) environments, but the most intense (cyclogenetic–unstable) cases deviate by ~12 hPa after 5 days, although the maximum low-level wind values are approximately the same for weak and strong initializations after 4 days. The storms initiated with the

weak and strong vortex initialization retain their relative storm size throughout the integrations. An analysis of the low-level storm force winds at 120 h in the six experiments of Fig. 4 reveals a mean extent of 228 and 468 km for the weak and strong vortex cases, respectively. Note that most experiments exhibit monotonic intensification in minimum surface pressure, but the low-level wind has more variation in time.

b. *Maximum intensity dependence*

The idealized experiments were run for 11 different thermal anomalies for each of 11 different SSTs, following the experimental design of SH00. The transient behavior of a selection of these experiments was discussed in the last section. For a more systematic analysis of the parameter space, maximum intensities for these 121 sets of environmental conditions are graphed in Fig. 5 for minimum surface pressure. A similar analysis of maximum 10-m winds was also completed and indicates complimentary results (not shown). Results are shown for both the strong (color shading) and weak (contours) initial vortex specification based on the minimum pressure during hours 12–120 of each integration. Note that the intensity behavior is fairly systematic over this parameter space despite analyzing a maximum, instantaneous quantity. Intensities range from about 975 to 915 and 905 hPa for the weak and strong vortex, respectively; the maximum 10-m winds range from ~35 to ~65 and 70 m s^{-1} for the weak and strong vortex, respectively. The intensity behavior observed in Fig. 4 holds for the entire parameter space in that the largest difference in minimum surface pressure between weak and strong initial vortex cases is for the more cyclogenetic environment (higher intensities). As seen previously, the overall pattern of intensity in Fig. 5 is similar to SH00, with both weak and strong initial vortex conditions resulting in a similar pattern, with the strongest storm cases being for cold upper anomalies and high SST. As shown previously for the GFDL 2014 model, the weak initial vortex specification yields higher-pressure storms relative to the strong vortex specification in the intense region of the SST–stability parameter space (~10 hPa), although the maximum 10-m winds are almost identical at the end of the 5-day integrations for weak and strong initial conditions. As can be inferred from Fig. 5, the maximum intensity (in hPa) is well correlated with SST and upper-air thermal anomalies for both strong and weak initial vortex conditions. The correlations between intensity and SST are 0.83 and 0.70 for the strong and weak initial conditions, respectively, across the 11 upper-level anomalies at each SST. The correlations between intensity and initial stability are 0.54 and 0.66 for the strong and weak initial conditions, respectively, for the 11 SST anomalies at each stability category.

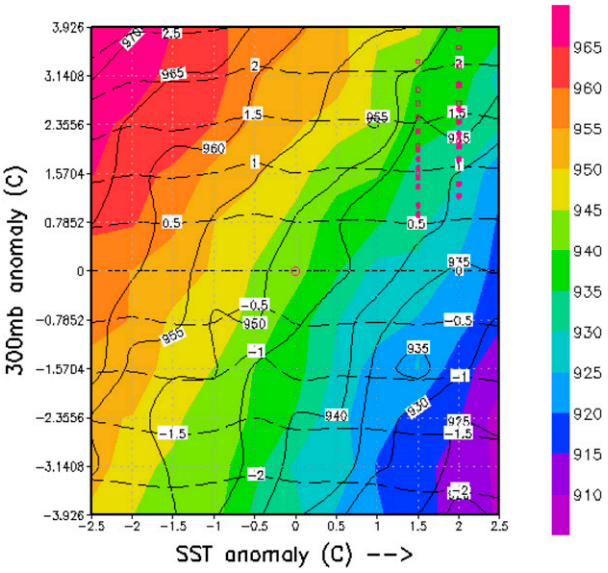

FIG. 5. Distribution of minimum sea level pressure for each model 120-h integration for the entire suite of experiments with 11 upper-air thermal anomalies (ordinate) and 11 SST anomalies (abscissa). Parameter space results are color shaded (910–965 hPa) for strong vortex cases and contoured (solid lines from 920 to 970 hPa) for weak vortex cases. Domain-averaged upper-level temperature anomalies (dashed lines from −2 to +2.5 K in 0.5-K increments) at 60 h relative to the control experiment are shown. Colored circles (squares) indicate upper-level warming values for various CMIP3 climate models at 1.5° and 2.0°C SST warming for initial (~60 h) warm anomalies. The control, no anomaly experiment is indicated by a small open red circle near the center of the figure.

As discussed earlier, the upper-level warm anomalies are free to evolve in time and indeed in these idealized experiments trend to a more radiative–convective equilibrium state. Interestingly, the thermal anomalies evolve in a consistent manner in the parameter space studied. Figure 5 (dashed lines) indicates that the anomalies at 60 h are roughly ~66% of the initial value but approximately independent of SST and thus qualitatively do not affect the conclusion that upper-level anomalies affect tropical cyclone intensity. Obviously, for more slowly developing storms in these experiments, Fig. 5 indicates that the stability may have even a larger impact than discussed above.

These results can be used to explore the contributions to projected TC intensity changes in global warming scenarios, although it is somewhat problematic since the upper warm anomalies change in time. For that reason, it is advantageous to analyze the suite of cases evolving from the strong vortex, since those cases reach their most intense state in ~60 h. Both initial and 60-h values of mean upper-level warming are used in the evaluations.

Most climate models exhibit a pronounced upper-tropospheric warming enhancement compared to the SST warming in the tropics. A fairly wide range of tropical upper-tropospheric warming magnitudes, per degree of surface warming, are simulated in global warming experiments with climate models (e.g., Knutson and Tuleya 2004), but typically the upper-tropospheric warming exceeds the surface warming by about a factor of 2 (Knutson and Tuleya 2004; Hill and Lackmann 2011). Upper-level warming values from various CMIP3 climate models are shown in Fig. 5, assuming both the initial and ~60-h thermal anomalies of the model. Assessing this impact of this stabilization effect in our experiments, for example, a net initial (60-h) warming of 4°C aloft coupled with a 2°C increase of SST leads to an intensity increase of ~−8 (−5) hPa in SLP; with a constant warming with height, a 2°C SST increase would lead to a ~−16 hPa increase of intensity. For environmental pressure of 1012 hPa, these correspond to about +12% (+7%) and +23% increases in central pressure deficit, respectively. Thus, the stabilization of the upper troposphere (warming enhanced by a factor of 2) reduces the TC intensification by up to 50% compared to a uniform warming with height. These sensitivity findings are broadly similar to those of SH00 and Hill and Lackmann (2011). Because of the spread among models in the degree of upper-tropospheric warming amplification, for a tropical SST warming of roughly 2°C, the sensitivity diagram suggests late-twenty-first-century TC intensity increases ranging from negligible to ~10 hPa, depending on the global climate model providing the projected climate changes and the relevant value of idealized model warming controlling the intensity. The amount of upper-level warming is still problematic in global warming scenarios (Vecchi et al. 2013). These results are broadly consistent with recent twenty-first-century climate change projection downscaling studies using the GFDL hurricane model in conjunction with various regional and global climate models (i.e., Knutson et al. 2013, 2015, Bender et al. 2010). On the other hand, some investigators (e.g., Lau et al. 2016), have adopted an approach of changing only SST and not changing atmospheric temperatures in their initial and boundary conditions for a dynamical TC downscaling experiments. Not surprisingly, this leads to dramatically larger intensification than simulated in our previous studies. However, we can infer from our parameter space results that the dramatic projected future TC intensification in Lau et al. (2016) is very likely due to their unrealistic treatment of the atmospheric temperature profile change.

c. *Comparison to SH00*

One can directly compare the result obtained here to that of SH00 for the same parameter space. The most direct comparison is for the 5 m s^{-1} results of SH00 (their Fig. 5) and that of the present experiment with 5 m s^{-1} flow and a strong specified initial vortex. The initial conditions for SH00 and the present model (strong vortex) are almost identical. Only the vortex specification system and forecast model are different. As shown in Table 1, the model differences are substantial, with notable increases in model resolution and other model upgrades. The comparison indicates that both the slope and magnitude of simulated intensities are remarkably similar between the two studies (Fig. 6), with the GFDL 2014 model exhibiting slightly stronger SST dependence and therefore a ~5-hPa greater range. This overall similarity may be the result of model development tuning toward realistic, small bias results, along with possible compensation between various physical and resolution changes.

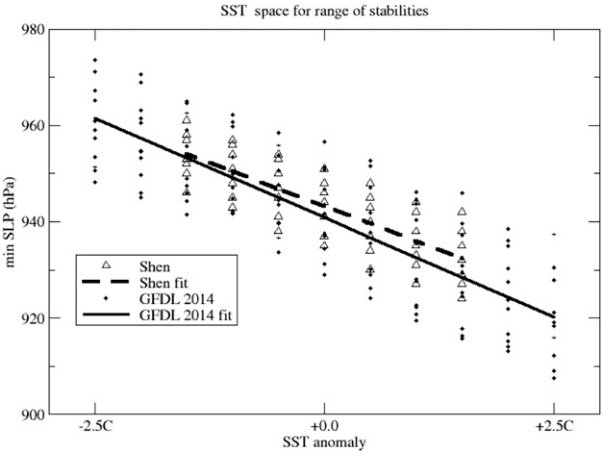

FIG. 6. Relationship between intensity (minimum SLP) and SST anomalies for experiments across a range of atmospheric stability changes for each SST anomaly value (black solid diamonds for GFDL 2014 with solid black line fit). The *x* axis has markers at −2.5°, 0.0°, and +2.5°C. The *y* axis extends from 900 to 980 hPa in increments of 20 hPa. SH00 (Shen) results are shown with open triangles and a dashed line for the fit to the data. Both lines depict linear regression fits.

One can also compare the atmospheric stability influence on intensity in the SH00 and GFDL 2014 model hurricane, as shown in Fig. 7. The results indicate both the slope and magnitude of intensity dependence are remarkably similar. The GFDL 2014 model results yield slightly deeper (~2 hPa) storms than their SH00 counterparts throughout the range of atmospheric stabilities. Overall, the intensity relationship to initially specified stability is quite similar between the SH00 and the GFDL 2014 models despite the many changes in the GFDL model in the past decade. Because of the linear nature exhibited between the SST and stability anomalies to intensity, one can do a simple linear regression as a good first-order approximation to the obtained

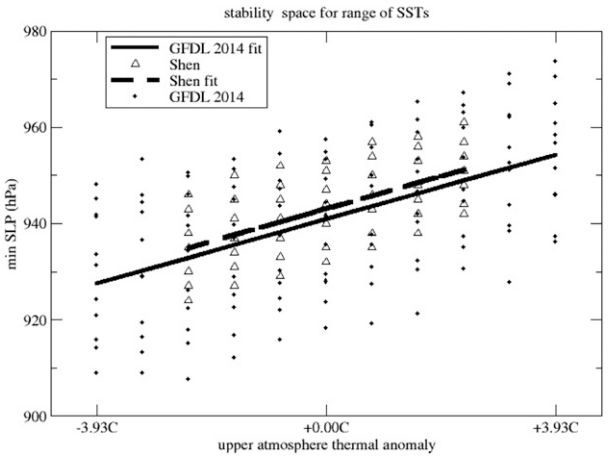

FIG. 7. As in Fig. 6, but for initial upper-air thermal anomalies for experiments across a range of SST anomalies for each upper-atmospheric thermal anomaly. The x axis has markers at −3.93°, 0.00°, and +3.93°C.

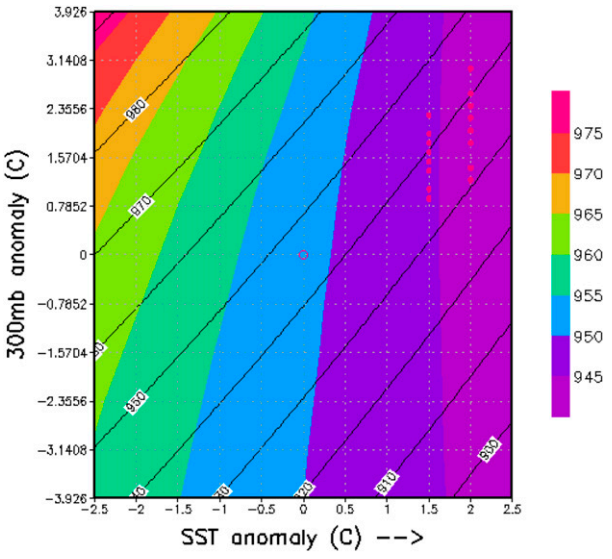

FIG. 8. Maximum potential intensity (Emanuel 1995, the 2013 version) for the same parameter space used by the suite of experiments for the 2014 idealized GFDL model (see Fig. 4). The x axis is from −2.5° to +2.5°C in increments of 0.5°C; and the y axis is from −3.926° to +3.926°C in increments of 0.7852°C. The color shaded values (from 945 to 975 hPa in increments of 5 hPa) are based on a formulation of PI that includes dissipative heating. The black contour (from 900 to 980 hPa in increments of 10 hPa) values are computed without dissipative heating effects and using environmental CAPE closure. The red filled dots indicate values for various CMIP3 climate models; the red open circle in the middle is the control case. See text for further details.

results: That is pgfdl = 949.6 − 4.1SSTI + 2.7STABI and pshen = 948.6 − 3.6SSTI + 2.7STABI, where pgfdl and pshen are the minimum central surface pressures (hPa), and SSTI and STABI are the SST and initial stability anomaly indices (1–11) of the experiments. These regressed results further confirm the close relationship between our present results and those of SH00 and the fact that the SST dependence of the GFDL 2014 model is slightly larger than that of SH00 (i.e., SSTI coefficient of 4.1 vs 3.6). Note that, since the thermal anomalies degrade in time, SH00 and the present study may underestimate the role of stability if one considers only the initially specified stability.

d. Comparison to maximum potential intensity

Our idealized model results can be compared to those obtained from the maximum potential intensity (PI) theory of Emanuel (1995) (see the 2013 version at ftp://texmex.mit.edu/pub/emanuel/TCMAX). Figure 8 shows that the Emanuel PI distribution has a smaller SLP range than either of the GFDL weak and intense vortex experiments (Fig. 5). Furthermore, the dependence of PI on upper-air anomalies is quite different from that of the GFDL model except for the weak intensity regions of the parameter space examined. For the parameter space as a whole, one sees that PI is mostly a function of SST and has a relatively weak dependence on tropospheric stability, as examined here, especially for relatively warm SSTs. For a sample global warming scenario consisting of ~1.5°C warming for SST combined with an upper-tropospheric warming of 3.0°C (1.5°C anomaly relative to the surface), from Fig. 8 one would expect an increase of intensity of ~6 hPa from the control intensity based on the PI, similar to the sensitivity to these changes in the GFDL model (Fig. 5). However, there are differences across the parameter space, as noted. The PI results may be sensitive to the initial height of thermal anomaly and assumed height of PI outflow layer. For example, Vecchi et al. (2013) present some sensitivity calculations illustrating the sensitivity of PI to changes of upper-tropospheric (mainly above 350 hPa) and tropopause transition layer (TTL) temperatures at 100 and 150 hPa, but this sensitivity is apparently different in detail from the GFDL model.

On the other hand, if one adopts Garner's (2015) environmental closure method in the PI formulation, the distribution and range of PI across the parameter space is more similar to the GFDL 2014 model results, especially if no dissipative heating is assumed (see line contours in Fig. 8). The GFDL model includes only some dissipative heating effects. These results are consistent with the results of SH00 in which the model intensity distribution is highly correlated with a metric they termed "hurricane CAPE." Of course, there are many differences between PI theory and the 2014

GFDL model, one being the role of the ocean shown in later sections and the appendix.

5. Impact on rainfall for range of SSTs and upper thermal anomalies

The relationship of area-mean storm total rainfall along the storm track (33.3° × 13.3° area) is similar to that of intensity, with high rainfall at high SSTs and cold upper anomalies for the parameter space studied for both weak and strong initial vortex cases. As in Fig. 5, colored dots/boxes in Fig. 9 indicate upper-level warming values for various CMIP3 climate models at 1.5° and 2.0°C SST warming for initial and ~60-h warm anomalies. Note that, in Fig. 9, the area-mean total rainfall sensitivity diagram shows a quite smooth dependence on SST and initial upper-tropospheric anomalies and is consistent for both strong (shaded) and weak (contours) vortex initializations. As in the intensity distribution, the storm total rainfall for the strong initial vortex case varies more than that with the weak vortex. This is in part because of the larger storm size and the higher storm intensities during the early storm stages of storm development with strong vortex initializations. In contrast, the maximum total rainfall in the storm area with either initialization (not shown) has more variation and has a stronger dependence on SST changes than on upper-tropospheric temperature anomalies (stability). The correlation with SST is 0.83 (0.90) and 0.80 (0.70) for the area-mean total and maximum total precipitation, respectively, for the weak (strong) initial vortex cases. The correlation with initial upper thermal anomalies is lower: 0.54 (0.43) and 0.40 (0.54) for the area-mean storm total and max total, respectively, for weak (strong) vortices. Therefore, the statistical robustness of the relationship between precipitation and SST is stronger than between intensity and SST, as evident in the higher correlations, though the opposite is true for the stability dependence. A linear regression was also performed with rainfall in addition to storm intensity, which also confirms these results. A key finding in Fig. 9 is that stability affects the precipitation rate (for a given SST) through its control on storm intensity. While the dependence of precipitation on SST alone may result from higher atmospheric water vapor content and increased storm intensity, at fixed SST the environmental water vapor may also be relatively unchanged. In that case, we speculate that the enhanced rainfall for fixed SST as the stability decreases may be a result of increased storm intensity, which enhances moisture convergence and evaporation rates even if the large-scale environmental water vapor content of the atmosphere does not increase (Tuleya et al. 2007). For a

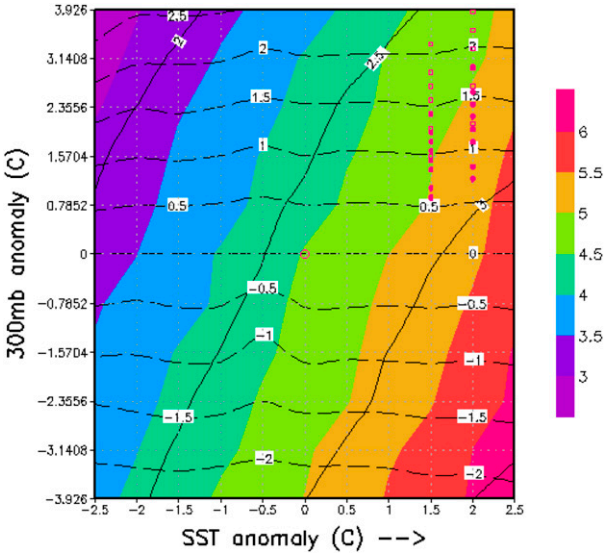

FIG. 9. As in Fig. 8, but for the distribution of area-mean storm total rainfall (cm) along the storm track (33.3° longitude × 13.3° latitude area) for the entire suite of experiments with 11 upper-air thermal anomalies and 11 SST anomalies. Parameter space results are color shaded (from 3 to 6 cm in increments of 0.5 cm) for strong vortex cases and contoured (solid black lines, from 2 to +3.5 cm in increments of 0.5 cm) for weak vortex cases. Domain-averaged upper-level temperature anomalies (dashed black lines, from −2° to +2.5°C in increments of 0.5°C) at 60 h relative to the control experiment are shown.

sample global warming scenario of ~1.5°C warming for SST combined with an upper-tropospheric warming of 1.5°C anomaly relative to the surface, from Fig. 9 one would expect an increase of ~0.3–0.5-cm (~8%–10%) average mean storm total rainfall based on the strong vortex cases, depending on whether one uses the initial anomaly or that estimated at 60 h. Most CMIP3 climate model upper-air thermal anomalies indicate increases in rainfall amount despite the transience in the model warm thermal anomalies. The strong relationship between rainfall and upper-level thermal anomalies still exists. Our results seem consistent with the global dynamical downscaling results of Knutson et al. (2015), in which rainfall increases for a warmer climate relatively more robustly across models and various regions than intensity increases for the global warming scenarios examined.

6. Impact of vertical shear on idealized storms

Vertical wind shear has a demonstrated effect on storm formation and demise [e.g., Gray (1968)]. A simple explanation is that when the warm core aloft is not aligned with the surface circulation because of the differential horizontal advection or the "ventilation

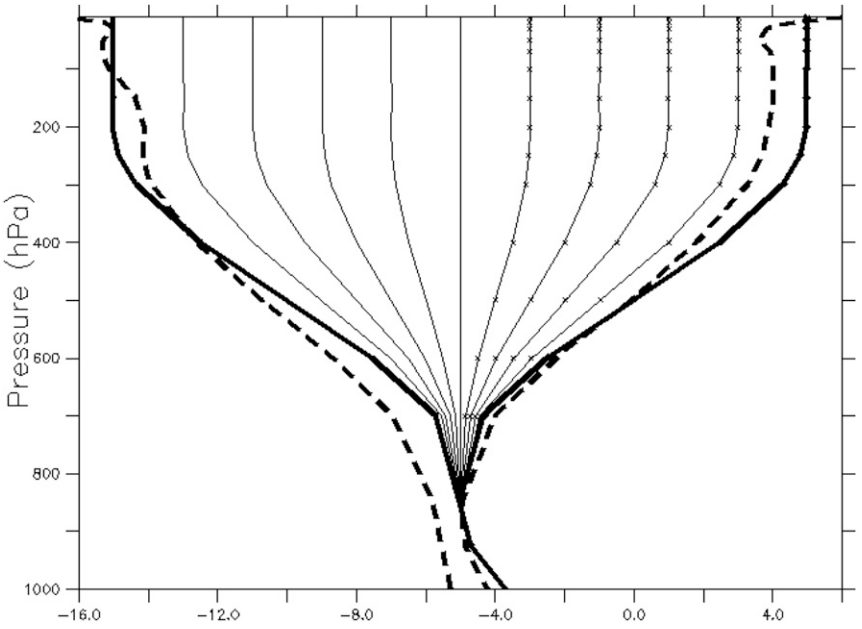

FIG. 10. Vertical shear wind profiles for the idealized experiments with maximum westerly wind shear ($10\,m\,s^{-1}$) patterned after WC04. In the suite of vertical shear experiments, vertical shear is incrementally changed in equal increments toward easterly shear ($-10\,m\,s^{-1}$). Wind in lower atmosphere is $\sim 5\,m\,s^{-1}$ easterly. Initial (60 h) values for extreme cases of $\pm 10\,m\,s^{-1}$ shear are shown by thick solid (dashed) lines. Other intermediate vertical shear initial conditions are shown by the thin lines.

effect'' (e.g., Tang and Emanuel 2012), drier air is brought into the storm core. Unlike the SST effect, environmental flow is complicated in observed cases and difficult to analyze and diagnose. Some vertical shear is regarded as conducive for development, such as outflow channels enhancing mass export from the core region. Examples of modeling studies analyzing the impact of shear include early work by Tuleya and Kurihara (1981) and more recently Frank and Ritchie (2001), WC04, Ritchie and Frank (2007), and Nolan and McGauley (2012). Operational hurricane prediction models, such as the GFDL hurricane model and the HWRF Model have not been analyzed in an ideal configuration to study vertical shear effects. Some early limited analyses of the operational GFDL model suggested that earlier versions of the GFDL model might not be sensitive enough to vertical shear. In the present study, we perform a suite of experiments for the same range of SST (−2.5° to +2.5°C) as in sections 4 and 5, but with systematic change in vertical wind shear instead of upper-tropospheric thermal anomaly. The shear sensitivity is studied based on the unidirectional shear profile used in WC04. The surface flow was kept constant at the $5\,m\,s^{-1}$ easterly flow used in the previous experiments in this study, but with the $10\,m\,s^{-1}$ shear profile of WC04 altered in a set of 11 experiments. The shears tested ranged from $10\,m\,s^{-1}$ westerly, reduced in equal increments to zero shear, then increased in equal increments to $10\,m\,s^{-1}$ easterly shear (Fig. 10). The surface flow is fixed to ensure that the surface flux is roughly the same initially for each experiment with different vertical shear. As in the stability experiments, the two initial vortex initializations were tested. In addition, some supplemental experiments were performed without ocean coupling. The shear anomalies in our experiments will obviously affect the deep-layer mean flow and thus storm propagation as well. The propagation and tracks movements will be discussed later. Analogous to the stability suite of experiments, the imposed initial shear was constrained only by the fixed lateral boundary conditions. In these experiments, there is little deviation from the original domain-averaged wind profiles at 60 h for the extreme easterly and westerly shear cases for the control SST, as shown by the dashed lines in Fig. 10.

a. Results for control SST

Modeled wind intensities for the 11 distinct vertical shear profiles using the control SST and the weak initial vortex specification (Fig. 11, upper curves) display a wide range of resultant intensities. The intensities are shown for hour 72, before any disturbances dissipate. There is a systematic variation of intensity with vertical

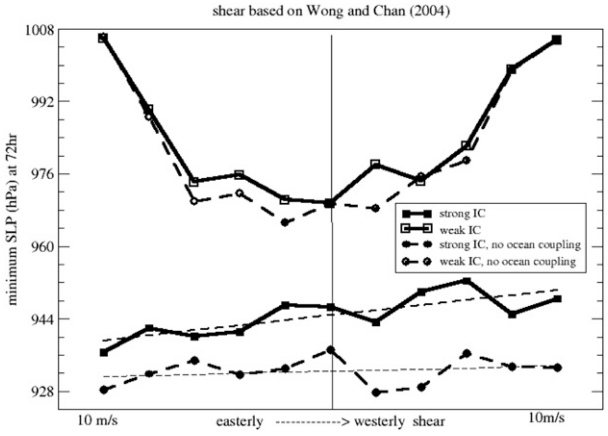

FIG. 11. Model intensity (minimum SLP) at 72 h for all 11 values of vertical shear anomaly for control SST with (squares) and without (circles) ocean coupling. Open (filled) squares and circles are for weak (strong) vortex initializations. The *x* axis ranges from -10 to $+10\,\mathrm{m\,s^{-1}}$ for easterly shear on the left and westerly on the right. The *y* axis is from 928 to 1008 hPa in increments of 16 hPa.

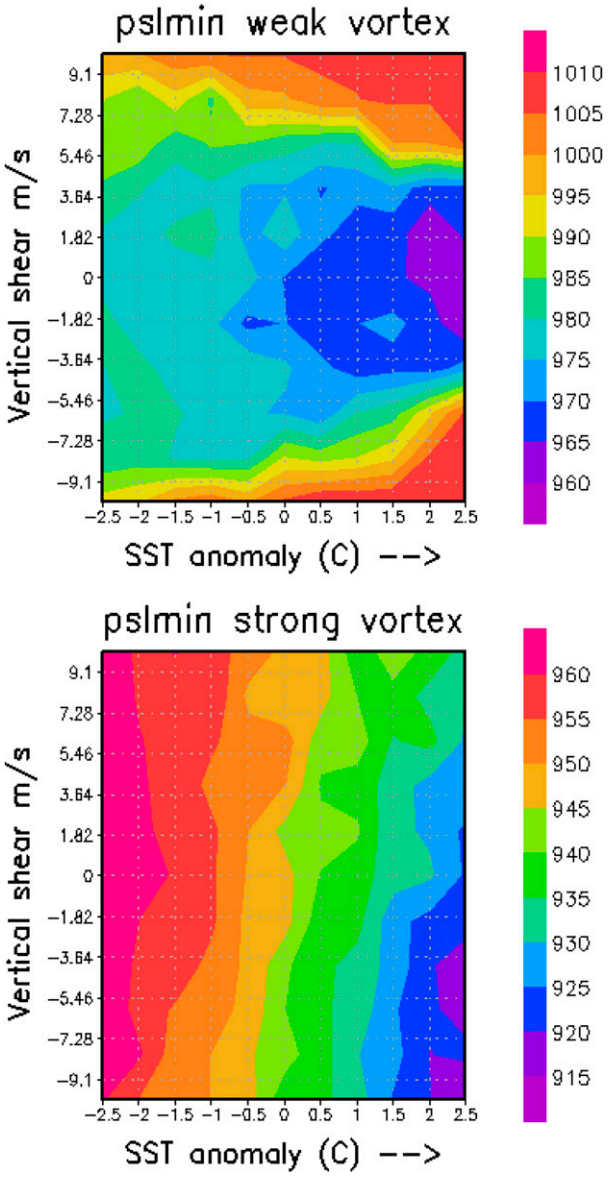

FIG. 12. Distribution of minimum SLP at 72 h of each model integration for the entire suite of experiments with 11 different vertical shears (ordinate; values from -9.1 to $+9.1\,\mathrm{m\,s^{-1}}$ in increments of $1.82\,\mathrm{m\,s^{-1}}$) and 11 SST anomalies (abscissa; values from $-2.5°$ to $+2.5°$C in increments of 0.5°C). Negative shear values indicate easterly vertical shear. (top) Weak and (bottom) strong initial vortex cases. Values of 1010 hPa are assigned to those cases that dissipated prior to 72 h.

shear with maximum intensity near zero shear, but with some bias for the highest intensity to occur for weak easterly vertical shear. This result is similar in some respects to earlier studies of Tuleya and Kurihara (1981), Frank and Ritchie(2001), and WC04. On the other hand, these results deviate from model results reported in Nolan and McGauley (2012). A caveat is that all of the above studies were different in initial conditions and experimental design. Also shown in Fig. 11 (upper curves) is the result with no ocean coupling for the weak vortex. Although the storm's cold wake may impact slower-moving westerly sheared systems to a larger extent, the impact of ocean coupling on the intensity response to shear is weak for this case. On the other hand, ocean coupling reduces the intensity of intense systems (e.g., weakly sheared in our case), with little impact on less developed, weak systems (Fu et al. 2014).

The response to vertical shear is different with the strong vortex initialization, Fig. 11 (lower curves). A rather moderate intensity difference (~12 hPa) occurs from westerly to easterly vertical shear for the control SST. With experiments run uncoupled for strong vortex initialization, the intensities are nearly independent of shear with strong vortex initialization. This indicates that the cold wake effect is more efficient for westerly sheared cases compared with easterly sheared cases since easterly sheared storms propagate faster.

b. Results for a range of SSTs with weak vortex initial condition

One can extend the results on vertical wind shear (Fig. 12) to the same range of SST anomalies (i.e., $-2.5°$ to $+2.5°$C) that were discussed earlier exploring the influence of stability on intensity and rainfall. To a large extent, the same relationship as for the control SST is found: weak shear leads to greater intensity. Interestingly at strong vertical shear, storms tend to decay more at high SST than at low SST. Across the 121 shear experiments, 10 storms dissipated during the 5-day integrations. The

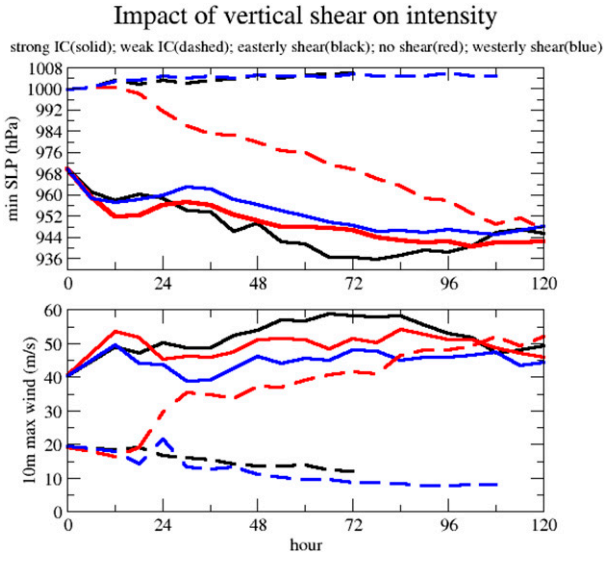

FIG. 13. Time history of (top) model minimum SLP and (bottom) maximum 10-m wind for three different vertical shears at the control SST. The easterly sheared ($-10\,\mathrm{m\,s^{-1}}$; black), zero vertical shear (red), and westerly vertical sheared ($+10\,\mathrm{m\,s^{-1}}$; blue) are shown for weak (strong) initial vortices by dashed (solid) lines. Both easterly and westerly sheared disturbances initiated with weak dissipating vortices.

cyclogenetic preference for weak easterly shear that is displayed in the control SST cases is more prevalent at cooler SSTs than at higher SSTs, where storms were more intense. Note that, at higher SST, storm intensity is more sensitive to vertical shear than at lower SST, with a wider range of simulated intensities (Fig. 12, top). As shown in Fig. 13, small sheared cases intensified ~50 hPa, with maximum winds exceeding $50\,\mathrm{m\,s^{-1}}$. Empirical evidence supports the notion that weak easterly vertical shear is more cyclogenetic than no shear [see review of observations in Nolan and McGauley (2012)]. Similar evidence appears in early model results in, for example, Tuleya and Kurihara (1981), and more recently in Ritchie and Frank (2007). Overall, the present idealized results with weak initial vortices support observational evidence as outlined by Gray (1968) and other lines of evidence that the shear is an important component of intensity, such as the operational Statistical Hurricane Intensity Prediction Scheme (SHIPS; DeMaria and Kaplan 1999).

c. *Vertical shear impacts with strong vortex initial condition*

The impact of vertical shear on storm intensity is different when the strong initial vortex of Fig. 3 is used. A set of 121 (11 × 11) experiments was performed for the same shear–SST parameter space as with the weak vortex initialization. However, none of the stronger initial disturbances dissipated when exposed to the same range of vertical shears as in the weak vortex cases (Fig. 12, bottom panel, and Fig. 13). Apparently, at least in the GFDL model system, a strong storm can persist even when subjected to substantial vertical shear. In contrast to the initialized weak system cases, where substantially sheared systems weakly develop or dissipate, there was little difference between the strong initial vortex systems, as they slowly deepened from ~966 hPa to below 950 hPa in the first 3 days of the simulations for the control or cold anomaly SST cases. During the first 3 days, there is tendency for more rapid development (~15 hPa) for easterly shear, as compared with the westerly sheared case for the control SST (Fig. 13). As seen in Fig. 12 (bottom), this preference for easterly sheared case development is more pronounced at high SST. As shown in section 6a, Fig. 11, the preference for easterly shear is mostly due to ocean coupling being more effective for slower-moving, westerly sheared systems. One can contrast the large differences between strong and weak initial disturbance behavior by analyzing Fig. 14 for the SST control case of strong westerly shear at 48 h. The weak disturbance case displays a 300-hPa warm core of ~3°C displaced downstream of the surface low pressure area with westerly flow immediately above the surface low. In contrast, the strong disturbance case displays a vertically stacked surface pressure, warm 300-hPa core of 13°C with strong cyclonic outflow. Westerly winds do not penetrate the warm core. A similar pattern for the easterly sheared cases exists (not shown). The strong initial disturbance cases show some qualitative similarity to the results of WC04 and Frank and Ritchie (2001) in that relatively intense storms are more resistant to vertical shear than weaker storms. However, the results of WC04 and Frank and Ritchie (2001) are not directly comparable to the present study for several reasons. For example, in previous studies the shear was imposed on a strong storm after an initial spinup period. Nevertheless, the inertially stable storm core of the strong initial model storm created in the GFDL axisymmetric spinup is apparently relatively impervious to shear. There remains a question whether this modeled behavior is an artifact, or whether, as seems true in the real world, stronger systems are more resistant to vertical shear influence (e.g., Zeng et al. 2008). Clearly, the shear sensitivity of the GFDL model storms is highly sensitive to the initial vortex chosen. While the weak initial vortex results appear physically consistent with empirical results and other model results showing that strong vertical shear is detrimental to storm development, our results indicate that the stronger initial vortex's development is relatively unaffected by the shear. This may result from the stronger vortex being more inertially stable and able to resist the environmental shear through vortex–flow interaction. The deep axisymmetric vortex developed in the GFDL vortex procedure (Kurihara et al. 1995) may have

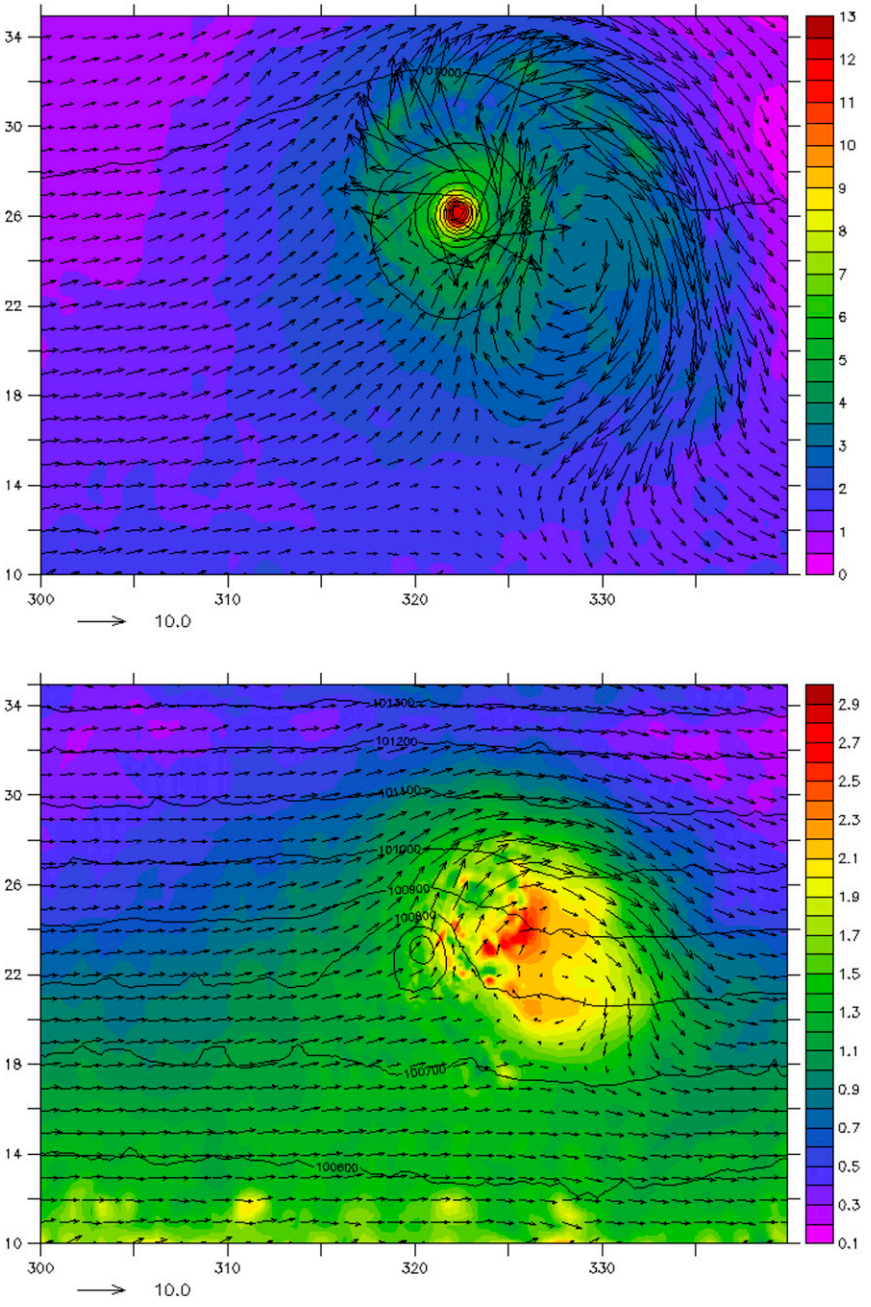

FIG. 14. The 300-hPa warm-core anomaly (°C, color shading) and wind ($m\,s^{-1}$, vectors with scale at bottom left of each panel) with surface pressure (contours labeled from 1008.00 to 1013.00 hPa in increments of 1.00 hPa) for (top) strong vortex and (bottom) weak vortex at 48 h at the control SST for westerly sheared cases (blue curves in Fig. 13).

some implications in that it may be too idealized and much less resistant to shear effects than a more complicated real initial condition. On the other hand, this robustness of results and insensitivity may be caused by the nature of the unidirectional shear imposed. In reality, vertical shear patterns are quite complicated in both the horizontal and vertical directions. As discussed in DeMaria (1996) and WC04, the intensity and size of the vortex, the Coriolis parameter, and the static stability of the atmosphere can all affect the magnitude of the vertical tilt of the storm and thus impact storm evolution.

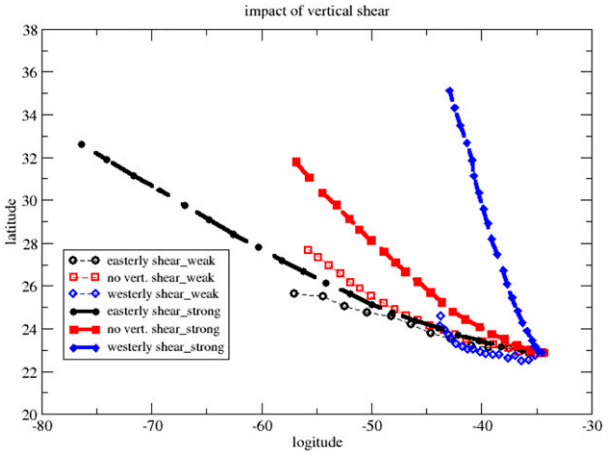

FIG. 15. Model disturbance tracks for six cases with distinct vertical shears and initial vortex strength: black circles for easterly shear, open for weak and closed for strong; red squares for no vertical shear, open for weak and closed for strong; and blue diamonds for westerly shear, open for weak and closed for strong. Note model simulations initiated with weak vortices and with either 10 m s^{-1} easterly or westerly vertical shears that dissipates before a full 5-day simulation.

d. Impacts of different vertical shears on model tracks

Figure 15 displays storm tracks in the six experiments for the highest westerly and easterly vertical shears and for the no-shear case, each using the control SST. Tracks for other SSTs showed similar behavior. Results are shown for both weak and strong initial vortex cases. The weak initial vortex (smaller) storms move westward and are influenced more by the zonal flow. The strong initial vortex (larger) storms are influenced more by the sheared flow aloft creating a latitudinal gradient of potential vorticity. Westerly sheared storms propagate slower and are influenced by the westerly flow aloft; easterly sheared storms propagate faster, supported by the stronger easterlies aloft. As mentioned earlier, the highly sheared storms dissipate during the 5-day forecast period for the weak initial vortex storms. Both the highly sheared [westerly (blue line) and easterly (black line)] cases dissipate during day 3 or 4.

On the other hand, the storms initiated with the strong vortex are highly robust and exist for the entire 5-day period, regardless of shear. As mentioned, the strong initial vortex case with westerly shear moved northwestward as the result of an enhanced beta effect induced by the westerly shear. The disturbance also increased in intensity from 966 to 944 hPa during its northward propagation. This westerly sheared system is somewhat comparable to the behavior of some operational model track and intensity forecasts of Tropical Storm Erika (2015), which had a northward bias when encountering westerly shear of ~12 m s^{-1} with overintensification in the high-resolution regional hurricane models (Bhatia and Nolan 2013). A detailed analysis of this behavior is beyond the scope of this study but may be related in part to an unrealistically strong initial vortex in a highly sheared environment. Of course, in this highly idealized environment, it is difficult to diagnose causes of model shortcomings from initial condition tests alone. At least in this highly idealized environment, significantly different results are obtained by simply using a different intensity for the initial condition.

7. Summary

This study revisits the sensitivity of hurricanes to environmental conditions using the GFDL hurricane system following upgrades in the 2000s, when both improvements to resolution and model physics were made. This transition has resulted in improvements to both track and intensity in operational GFDL model forecasts. One question examined here is how these model changes affect the model's sensitivity to some basic environmental parameters known to influence intensity. This question is relevant for both operational forecasting and climate change applications of the model. The paper serves as a follow-up to SH00, which systematically examined the joint influence of upper-air anomalies and SSTs on storm intensity. The recent (2014) version of the GFDL hurricane system is run under idealized conditions for a wide range of SSTs, stabilities (upper-air thermal anomalies), and unidirectional vertical shears (westerly through easterly). The results from the stability suite of experiments were consistent with those of SH00 to a large extent despite significant improvements in model physics and increased vertical and horizontal resolution. A wide range of intensities resulted (905–980-hPa minimum SLP) for both strong and weak vortex initializations. The behavior of modeled intensity within the SST–upper thermal anomaly parameter space is almost identical to SH00, which used a GFDL hurricane modeling system circa ~1999. As in SH00, a climate model warming scenario in which the upper troposphere warms relative to the surface warming will offset a significant amount of the effect of surface warming alone on intensity. It was discovered in this study (and apparently in SH00) that the initially specified warm anomalies degrade by ~33% in 60 h throughout the parameter space as they gravitate toward the moist adiabat in this experimental framework. Nevertheless, significant anomalies persist for days, which strongly impacts intensity, although the stabilization effect may be underestimated if one considers the initial anomalous value alone. The stabilization of the upper troposphere projected by climate models (upper-tropospheric warming enhanced by roughly a factor of 2 compared to surface warming) reduces the TC intensification up to about 50% compared to a uniform warming with height. Nonetheless, for typical

late-twenty-first-century climate change scenarios, the upper-tropospheric warming does not completely negate the surface warming effect, and we simulate a net intensification of TCs by up to about 5–8 hPa or 7%–12% (central pressure deficit), which would correspond to about a 5%–9% increase in maximum wind speed, consistent with previous high-resolution dynamical model findings. PI theory indicates a similar relationship of intensity to SST anomalies. On the other hand, the GFDL model and PI theory have different sensitivities to upper-air temperature anomalies, at least for most areas in the SST–stability parameter space examined in this study. Some of this difference may be due to the closure assumption in PI theory.

Simulated tropical cyclone rainfall was also investigated over the SST–stability parameter space using our idealized experimental design. Area-mean total rainfall increases with SST warming and associated upper-tropospheric warming, consistent with previous climate change studies using the GFDL model for downscaling storm cases (e.g., Knutson et al. 2013, 2015). We show that storm total rainfall can also increase, for fixed SST, if the upper troposphere cools (stability decreases). Thus, consistently in our experiments, tropical cyclone rainfall increases with storm intensity, whether because of SST or stability changes. For global warming scenarios, overall impact on stability on rainfall may be underestimated if one considers only the initially specified warm anomalies that tend to degrade in time in this idealized setting. This does not influence the strong qualitative relationship found between stability and SST on storm rainfall in this study.

The GFDL 2014 forecast system sensitivity to vertical shear was also investigated in a systematic set of idealized experiments. The model dissipated weak initial disturbances under both strong easterly and strong westerly shear of $10\,\mathrm{m\,s^{-1}}$. A small but noticeable tendency for stronger storms with easterly sheared versus westerly sheared environments was found at lower values of SST. The impact of vertical shear on intensity was different when a strong vortex was initiated in the GFDL forecast system. In this case, none of the initial disturbances weakened; furthermore, most intensified at least to some extent and were dependent on SST. Apparently, the strong initial disturbance was sufficiently robust to be essentially impervious to the detrimental effects of vertical shear as applied here. Furthermore, westerly sheared systems were not as intense as easterly sheared system at high SST because of the retarding effect of the wake for slowly moving, westerly sheared systems. In the westerly sheared case, a strong system moved northward, impacted by the strong westerlies aloft. Interestingly, this phenomenon appears quite similar to spurious forecast behavior of the GFDL operational systems when storms are impacted by significant westerly shear. However, this anomalous idealized behavior can only be confirmed in the operational setting with more in-depth analysis of case studies of observed systems using the GFDL forecast system.

Acknowledgments. The authors thank Steve Garner and David Nolan for reviewing an earlier version of this transcript and for their many constructive comments. The authors would also like to thank the three anonymous reviewers for their comments and criticism as well. The senior author would like to thank the GFDL community for support extending well after his retirement through NOAA Contract EA133R-13-BA-0045. Coauthors IG and BT were supported by a grant from WeatherPredict Consulting, Inc., an affiliate of RenaissanceRe.

APPENDIX

Impact of Different Warmed Ocean Profiles

The main emphasis of this paper is to study the sensitivity of model storm intensity and rainfall to changes in atmospheric stability and vertical shear. On the other hand, storm intensity is highly sensitive to SST and the underlying ocean. For the main body of this paper, the ocean was initiated with a climatological (GDEM) averaged profile adjusted for any specified anomalies in SST. The upper-ocean temperature is modified by assimilating the adjusted SST (i.e., observed or from a global warming experiment) in the control GDEM profile, the URI method of initialization as described in Yablonsky and Ginis (2008) and Yablonsky et al. (2015a). In this SST assimilation procedure, the mixed-layer depth remains nearly the same as the control profile, regardless of the SST imposed, and the ocean subsurface temperature is tapered toward original climatology below the mixed layer. This is the same method utilized in the operational GFDL hurricane forecast model and in the climate change downscaling study of Knutson et al. (2015) to insure that the ocean subsurface temperatures are consistent with the SSTs obtained from either observations (for forecast runs) or climate models (for global warming impact studies). As the result of the assimilation procedure, there is an increased vertical temperature gradient below the mixed layer in global warming cases. This method was used in Knutson et al. (2015) instead of using the ocean temperature changes with depth obtained directly from the CMIP5 models because the CMIP5 model ocean data existed only on a variety of specialized model-specific irregular grids, which were very difficult to work with, as opposed to more workable latitude–longitude grids.

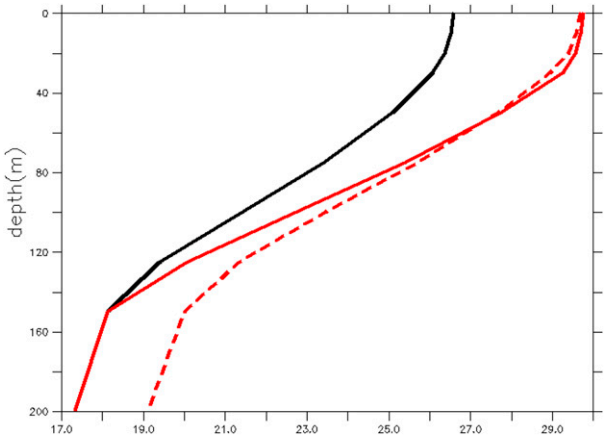

FIG. A1. Initial oceanic temperature profiles for MDR Atlantic region used in supplementary idealized study: control profile of H15 (black); warm profile of H15 (red dashed); warm profile using URI mixing method (red solid). The *y* axis increases from a depth of 0 to 200 m in increments of 20 m. The *x* axis ranges from 17.0° to 29.0°C in increments of 1.0°C.

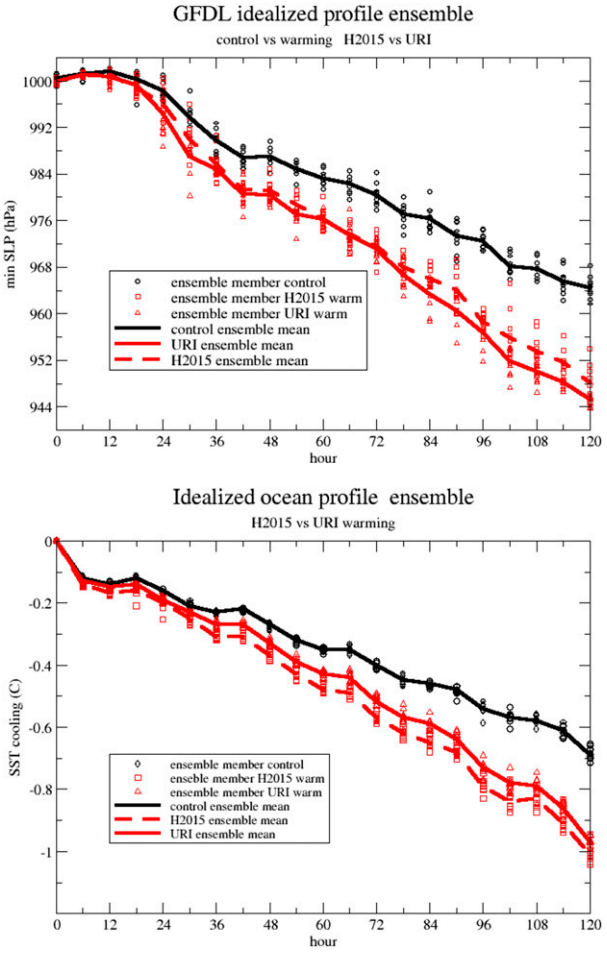

FIG. A2. (a) GFDL idealized intensity evolution of intensity (hPa) for a 10-member ensemble for MDR Atlantic region: control profile of H15 (black line and open circles); warmed profile of H15 (red open squares); warm profile using URI mixing method (red open triangles). The URI ensemble mean is represented by a solid red line. The H15 ensemble mean is represented by a dashed red line. (b) As in (a), but GFDL idealized evolution of SST cooling in wake area.

A recent study of H15 has noted that, for specific tropical cyclone main development regions of the world, including the tropical North Atlantic, the ocean's vertical temperature gradient is increased to some extent for global warming scenarios. H15 further suggest that the conventionally computed PI increase in global warming scenarios could be largely negated as a result of the increased cooling in the wake of tropical cyclones in warming scenarios. To test this result using a dynamical modeling framework, we performed a series of sensitivity experiments using the GFDL 2014 idealized model design as in the main part of this paper and the control and warmed initial profiles of H15 (their Fig. 1e). For the supplemental experiments, three initial ocean profiles were used: 1) the control profile of H15 for the Atlantic MDR; 2) the warmed profile of H15 for the Atlantic MDR; and 3) a warmed profile (URI profile) obtained by assimilating the same warmed SST as H15 in the control profile by the assimilation method mentioned in the above paragraph (Fig. A1). The URI profile is better mixed than the warmed profile of H15 in the upper 40 m of the ocean, having less stratification and a deeper mixed layer. Below that, the temperature of the URI profile tapers toward the original control values at 150 m, enhancing the sub-mixed-layer stratification over and above that of H15.

A 10-member ensemble was integrated for each of these initial ocean profiles. The ensemble suite of experiments was run in order to ensure robustness of the modeled intensity results. A random 0–1 m s^{-1} variation of the target maximum wind of the weak vortex of this paper was utilized to generate 10 members. In our experiments, the atmospheric profiles were adjusted to match the SSTs given by H15. Figure A2a summarizes the results of the 5-day integrations using the three ocean temperature profiles. Note that the H15 warm profile cases after 5 days were ~16 hPa more intense than those with the control profile. In comparison, the cases with the URI adjusted warm profile were ~20 hPa more intense than those utilizing the control profile. The warmed profile intensities from the H15 and URI methodology are clearly distinct from the control case intensities. Although there is overlap among the individual warmed ensemble members of the H15 and URI warmed profile cases, it appears that the use of the H15 warmed profile instead of the URI profile leads to a slight reduction in

the climate change–induced intensification of TCs in the model. This is demonstrated here for the idealized GFDL modeling system and the initial conditions used and is the result of the reduced mixed-layer depth in the H15 profile. Emanuel's (2015) analysis of mixed-layer depth changes in the CMIP5 models shows that the decrease in mean mixed-layer depth is not a robust result across all of the CMIP5 models. The intensity results shown here are consistent with the ocean cooling analyzed in the wake behind the idealized model storm for each of these three experimental suites in Fig. A2b. Both cases with warmed profiles exhibit stronger cooling, but more intense storms, than the control cases. The H15 profile cases display more TC-induced SST cooling than the URI initialized profiles, which leads to up to ~20% less intensification than for the URI profile cases.

Thus, according to our experiments, the climate change sensitivity results in Knutson et al. (2015) may slightly overestimate the increased intensification of tropical cyclones by their use of the URI initialization method for their experiments, as opposed to the full ocean temperature profile changes from the CMIP5 models. However, this result depends on a reduced mixed-layer depth under climate warming, which is not a robust finding across all CMIP5 models. The amount of impact would, of course, also depend on the stratification of the particular CMIP5 model at the incipient TC location. These findings overall are similar to those of Emanuel (2015), who also reported that increased mixing in the cold wake behind TCs in global warming scenarios might slightly moderate the simulated TC intensity increases under climate warming conditions but would not eliminate the increased intensity.

REFERENCES

Bender, M. A., I. Ginis, R. E. Tuleya, B. Thomas, and T. Marchok, 2007: The operational GFDL coupled hurricane–ocean prediction system and a summary of its performance. *Mon. Wea. Rev.*, **135**, 3965–3989, doi:10.1175/2007MWR2032.1.

——, T. R. Knutson, R. E. Tuleya, J. J. Sirutis, G. A. Vecchi, S. T. Garner, and I. M. Held, 2010: Modeled impact of anthropogenic warming on the frequency of intense Atlantic hurricanes. *Science*, **327**, 454–458, doi:10.1126/science.1180568.

Bhatia, K. T., and D. S. Nolan, 2013: Relating the skill of tropical cyclone intensity forecasts to the synoptic environment. *Wea. Forecasting*, **28**, 961–980, doi:10.1175/WAF-D-12-00110.1.

Cheung, K. W., 2004: Large-scale environmental parameters associated with tropical cyclone formations in the western North Pacific. *J. Climate*, **17**, 466–484, doi:10.1175/1520-0442(2004)017<0466:LEPAWT>2.0.CO;2.

DeMaria, M., 1996: The effect of vertical shear on tropical cyclone intensity change. *J. Atmos. Sci.*, **53**, 2076–2087, doi:10.1175/1520-0469(1996)053<2076:TEOVSO>2.0.CO;2.

——, and J. Kaplan, 1999: An updated Statistical Hurricane Intensity Prediction Scheme (SHIPS) for the Atlantic and eastern North Pacific basins. *Wea. Forecasting*, **14**, 326–337, doi:10.1175/1520-0434(1999)014<0326:AUSHIP>2.0.CO;2.

——, J. A. Knaff, and B. H. Connell, 2001: A tropical cyclone genesis parameter for the tropical Atlantic. *Wea. Forecasting*, **16**, 219–233, doi:10.1175/1520-0434(2001)016<0219:ATCGPF>2.0.CO;2.

Emanuel, K., 1995: Sensitivity of tropical cyclones to surface exchange coefficients and a revised steady-state model incorporating eye dynamics. *J. Atmos. Sci.*, **52**, 3969–3976, doi:10.1175/1520-0469(1995)052<3969:SOTCTS>2.0.CO;2.

——, 2007: Quasi-equilibrium dynamics of the tropical atmosphere. *The Global Circulation of the Atmosphere*, T. Schneider and A. H. Sobel, Eds., Princeton University Press, 385 pp.

——, 2015: Effect of upper-ocean evolution on projected trends in tropical cyclone activity. *J. Climate*, **28**, 8165–8170, doi:10.1175/JCLI-D-15-0401.1.

Frank, W. M., and E. A. Ritchie, 2001: Effects of vertical wind shear on the intensity and structure of numerically simulated hurricanes. *Mon. Wea. Rev.*, **129**, 2249–2269, doi:10.1175/1520-0493(2001)129<2249:EOVWSO>2.0.CO;2.

——, and ——, 2002: Tropical cyclones in complex vertical shears. *Extended Abstracts, 25th Conf. on Hurricanes and Tropical Meteorology*, San Diego, CA, Amer. Meteor. Soc., 7C.1. [Available online at https://ams.confex.com/ams/25HURR/techprogram/paper_36346.htm.]

Fu, H. L., X. Wang, P. C. Chu, X. Zhang, G. Han, and W. Li, 2014: Tropical cyclone footprint in the ocean mixed layer observed by Argo in the Northwest Pacific. *J. Geophys. Res. Oceans*, **119**, 8078–8092, doi:10.1002/2014JC010316.

Garner, S. T., 2015: The relationship between hurricane potential intensity and CAPE. *J. Atmos. Sci.*, **72**, 141–163, doi:10.1175/JAS-D-14-0008.1.

Gopalakrishnan, S. G., F. Marks, X. Zhang, J. W. Bao, K. S. Yeh, and R. Atlas, 2011: The experimental HWRF system: A study on the influence of horizontal resolution on the structure and intensity changes in tropical cyclones using an idealized framework. *Mon. Wea. Rev.*, **139**, 1762–1784, doi:10.1175/2010MWR3535.1.

Gray, W. M., 1968: Global view of the origin of tropical disturbances and storms. *Mon. Wea. Rev.*, **96**, 669–700, doi:10.1175/1520-0493(1968)096<0669:GVOTOO>2.0.CO;2.

——, 1998: The formation of tropical cyclones. *Meteor. Atmos. Phys.*, **67**, 37–69, doi:10.1007/BF01277501.

Hill, K. A., and G. M. Lackmann, 2011: The impact of future climate change on TC intensity and structure: A downscaling approach. *J. Climate*, **24**, 4644–4661, doi:10.1175/2011JCLI3761.1.

Huang, P., I.-I. Lin, C. Chou, and R. Huang, 2015: Change in ocean subsurface environment to suppress tropical cyclone intensification under global warming. *Nat. Commun.*, **6**, 7188, doi:10.1038/ncomms8188.

Knutson, T. R., and R. E. Tuleya, 2004: Impact of CO_2-induced warming on simulated hurricane intensity and precipitation: Sensitivity to the choice of climate model and convective parameterization. *J. Climate*, **17**, 3477–3495, doi:10.1175/1520-0442(2004)017<3477:IOCWOS>2.0.CO;2.

——, ——, and Y. Kurihara, 1998: Simulated increase of hurricane intensities in a CO_2-warmed climate. *Science*, **279**, 1018–1020, doi:10.1126/science.279.5353.1018.

——, and Coauthors, 2013: Dynamical downscaling projections of 21st century Atlantic hurricane activity: CMIP3 and CMIP5 model-based scenario. *J. Climate*, **26**, 6591–6617, doi:10.1175/JCLI-D-12-00539.1.

——, J. J. Sirutis, M. Zhao, R. E. Tuleya, M. A. Bender, G. A. Vecchi, G. Villarini, and D. Chavas, 2015: Global projections of intense tropical cyclone activity for the late twenty-first century from dynamical downscaling of CMIP5/RCP4.5 scenarios. *J. Climate*, **28**, 7203–7224, doi:10.1175/JCLI-D-15-0129.1.

Kurihara, Y., and R. E. Tuleya, 1974: Structure of a tropical cyclone developed in a three-dimensional numerical simulation model. *J. Atmos. Sci.*, **31**, 893–919, doi:10.1175/1520-0469(1974)031<0893:SOATCD>2.0.CO;2.

——, G. J. Tripoli, and M. A. Bender, 1979: Design of a movable nested-mesh primitive equation model. *Mon. Wea. Rev.*, **107**, 239–249, doi:10.1175/1520-0493(1979)107<0239:DOAMNM>2.0.CO;2.

——, M. A. Bender, R. E. Tuleya, and R. Ross, 1995: Improvements in the GFDL hurricane prediction system. *Mon. Wea. Rev.*, **123**, 2791–2801, doi:10.1175/1520-0493(1995)123<2791:IITGHP>2.0.CO;2.

——, R. E. Tuleya, and M. A. Bender, 1998: The GFDL hurricane prediction system and its performance in the 1995 hurricane season. *Mon. Wea. Rev.*, **126**, 1306–1322, doi:10.1175/1520-0493(1998)126<1306:TGHPSA>2.0.CO;2.

Lau, W. K. M., J. J. Shi, W. K. Tao, and K. M. Kim, 2016: What would happen to Superstorm Sandy under the influence of a substantially warmer Atlantic Ocean? *Geophys. Res. Lett.*, **43**, 802–811, doi:10.1002/2015GL067050.

McClung, T., 2012: Amended: GFDL Hurricane Prediction System changes: Effective May 29, 2012. NWS Tech. Implementation Notice 12–18, 1 pp. [Available online at http://www.nws.noaa.gov/os/notification/tin12-18gfdl_aaa.htm.]

Nolan, D. S., and M. G. McGauley, 2012: Tropical cyclogenesis in wind shear: Climatological relationships and physical processes. *Cyclones: Formation, Triggers, and Control*, K. Oouchi and H. Fudeyasu, Eds., Nova Science Publishers, 1–34.

Ritchie, E. A., and W. M. Frank, 2007: Interactions between simulated tropical cyclones and an environment with a variable Coriolis parameter. *Mon. Wea. Rev.*, **135**, 1889–1905, doi:10.1175/MWR3359.1.

Shen, W., R. E. Tuleya, and I. Ginis, 2000: A sensitivity study of the thermodynamic environment on GFDL model hurricane intensity: Implications for global warming. *J. Climate*, **13**, 109–121, doi:10.1175/1520-0442(2000)013<0109:ASSOTT>2.0.CO;2.

Tang, B., and K. Emanuel, 2012: A ventilation index for tropical cyclones. *Bull. Amer. Meteor. Soc.*, **93**, 1901–1912, doi:10.1175/BAMS-D-11-00165.1.

Tuleya, R. E., and Y. Kurihara, 1981: A numerical study on the effects of environmental flow on tropical storm genesis. *Mon. Wea. Rev.*, **109**, 2487–2506, doi:10.1175/1520-0493(1981)109<2487:ANSOTE>2.0.CO;2.

——, M. DeMaria, and R. J. Kuligowski, 2007: Evaluation of GFDL and simple statistical model rainfall forecasts for U.S. landfalling tropical storms. *Wea. Forecasting*, **22**, 56–70, doi:10.1175/WAF972.1.

Vecchi, G. A., S. Fueglistaler, I. M. Held, T. R. Knutson, and M. Zhao, 2013: Impacts of atmospheric temperature trends on tropical cyclone activity. *J. Climate*, **26**, 3877–3891, doi:10.1175/JCLI-D-12-00503.1.

Williams, E., and N. Renno, 1993: An analysis of the conditional instability of the tropical atmosphere. *Mon. Wea. Rev.*, **121**, 21–36, doi:10.1175/1520-0493(1993)121<0021:AAOTCI>2.0.CO;2.

Wong, M. L., and J. C. L. Chan, 2004: Tropical cyclone intensity in vertical wind shear. *J. Atmos. Sci.*, **61**, 1859–1876, doi:10.1175/1520-0469(2004)061<1859:TCIIVW>2.0.CO;2.

Yablonsky, R. M., and I. Ginis, 2008: Improving the ocean initialization of coupled hurricane–ocean models using feature-based data assimilation. *Mon. Wea. Rev.*, **136**, 2592–2607, doi:10.1175/2007MWR2166.1.

——, ——, B. Thomas, V. Tallapragada, D. Sheinin, and L. Bernardet, 2015a: Description and analysis of the ocean component of NOAA's operational Hurricane Weather Research and Forecasting (HWRF). *J. Atmos. Oceanic Technol.*, **32**, 144–163, doi:10.1175/JTECH-D-14-00063.1.

——, ——, and ——, 2015b: Ocean modeling with flexible initialization for improved coupled tropical cyclone–ocean model prediction. *Environ. Modell. Software*, **67**, 26–30, doi:10.1016/j.envsoft.2015.01.003.

Zeng, Z., L. Chen, and Y. Yuqing Wang, 2008: An observational study of environmental dynamical control of tropical cyclone intensity in the Atlantic. *Mon. Wea. Rev.*, **136**, 3307–3322, doi:10.1175/2008MWR2388.1.

Zhang, D.-L., and E. Altshuler, 1999: The effects of dissipative heating on hurricane intensity. *Mon. Wea. Rev.*, **127**, 3032–3038, doi:10.1175/1520-0493(1999)127<3032:TEODHO>2.0.CO;2.